Coexistence of nonlinear states with different polarizations in a Kerr resonator

Tianye Huang,[1,2,*] Hongbo Zheng,[1,2] Gang Xu,[3] Jianxing Pan,[1] Fan Xiao,[1] Wufeng Sun,[4] Keda Yan,[4] Shaoxiang Chen,[5] Bao Huang,[6] Yu Huang,[7] and Perry Ping Shum[8]

[1]*School of Mechanical Engineering and Electronic Information, China University of Geosciences (Wuhan), Wuhan 430074, China*
[2]*Shenzhen Research Institute of China University of Geosciences, Shenzhen 518052, China*
[3]*School of Optical and Electronic Information, Huazhong University of Science and Technology, Wuhan 430074, China*
[4]*Optics Valley Technology Co., Ltd., Wuhan 430070, Hubei, China*
[5]*Wuhan Huaray Precision Laser Co. Ltd., Wuhan 430223, China*
[6]*Wuhan Raycus Fiber Laser Technologies Co. Ltd., Wuhan 430000, China*
[7]*Fiberhome Fujikura Optic Technology Co. Ltd., Wuhan 430070, China*
[8]*Department of Electronic and Electrical Engineering, South University of Science and Technology, Shenzhen 518055, China*

(Received 18 September 2023; accepted 8 November 2023; published 4 January 2024)

Temporal cavity solitons are optical pulses that can persist in passive resonators, such as microresonators and fiber-based resonators. They can preserve their shape and energy during the propagation. In addition, other typical nonlinear states including Turing rolls, chaotic state, and breathers also emerge in the Kerr resonator. Normally, the occurrence of these states is not simultaneous due to their distinct parameter regimes. However, their coexistence has been observed in scenarios where neighboring resonances corresponding to both the same and orthogonal polarizations partially overlap. The coexisting nonlinear states in the strongly birefringent resonator have not been thoroughly explored due to the challenge of superimposing multiple resonances. In this paper, we investigate the feasibility of inducing coexistence states within a strongly birefringent fiber ring resonator exhibiting anomalous dispersion. The dynamic effects are discussed in the context of zero and nonzero net birefringence. By flexibly controlling the overlap of the nonlinear resonances corresponding to two orthogonal polarizations, we can attain the coexistence of both homogeneous (two polarizations exhibit the same states) and inhomogeneous states (two polarizations exhibit different states). These results could have significant implications for high-compacity optical communication, LiDAR, dual-comb spectroscopy, and so on.

DOI: 10.1103/PhysRevA.109.013503

I. INTRODUCTION

Temporal cavity solitons (CSs) are optical pulses sitting atop a continuous wave (cw) background; they manifest themselves in the frequency domain as optical frequency combs (OFCs) with a series of equidistant spectral lines. They are special dissipative solitons that are able to recirculate indefinitely in the resonator without changes in shape or energy. The formation of the CSs results from a double balance between losses and parametric gain, as well as Kerr nonlinearity and chromatic dispersion. Optical Kerr microresonators with ultrahigh Q value are viewed as ideal platforms for the generation of CSs due to the capability of strong energy accumulation. In 2014, temporal CSs were first experimentally observed in a MgF_2 microresonator by Herr *et al.* [1], and thereafter soon demonstrated in the microresonators made up of various nonlinear materials, such as SiN [2], AlN [3], SiO_2 [4], etc. Temporal CSs exhibit strong stability in shape, velocity, and intensity during propagation, and their spectra are broad and strictly equidistant. The soliton frequency combs have demonstrated applications including high-precision frequency synthesis and measurement [5], distance measurement and light detection and ranging (LiDAR) [6,7], frequency calibration of astronomical spectrographs [8], optical atomic clocks [9], high-speed optical communications [10], and optical dual-comb spectroscopy [11]. Apart from microresonators, fiber-based resonators also serve as platforms for generating cavity solitons, including both Fabry-Perot (F-P) resonators [12] and macroscopic fiber ring resonators [13]. The former is fabricated by coating the end facets of the optical fiber with highly reflective Bragg mirrors, which have high finesse and repetition rates. As a comparison, the macroscopic fiber ring resonators correspond to the longer round-trip time and lower finesse. However, the meter-scaled cavity length contributes to a more flexible control of the physical characteristics, such as dispersion management [14,15], operating bandwidth [16], combined gain [17–19], synthetic dimension [20], and spatial parabolic potential [21].

Besides the CS state, the Kerr resonators with anomalous dispersion can also sustain other typical nonlinear states including Turing rolls, chaotic state, and breathers. It is worth noting that recent investigations have shown that the chaotic state has significant applications in LiDAR [22] and random number generators [23]. One increasing interest in the Kerr-cavity-based physical phenomenon is the coexistence of distinct nonlinear states originated from the partial overlap of the adjacent resonances [24]. This could be of applied relevance to the generation of multiplexed OFCs. Compared to a single polarization, the coexistence of nonlinear states in two

*tianye_huang@163.com

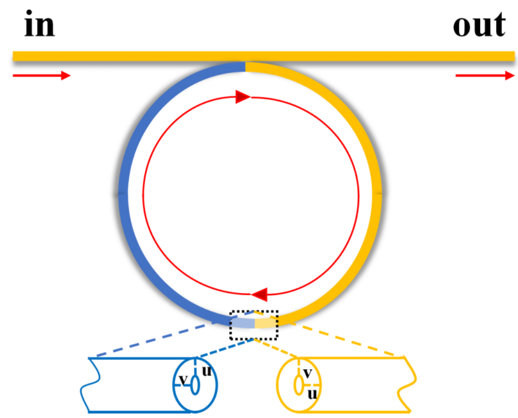

FIG. 1. Schematic diagram of the fiber ring resonator, where the fast axis (u) is aligned to the slow axis (v) at each spliced interface.

orthogonal polarizations has highly manipulating freedom and can be simply separated by the extracavity polarization splitting. Nielsen *et al.* reported the coexistence of two different polarization CSs in a weakly birefringent fiber resonator, but the driven strengths of the two polarizations are unbalanced [25]. The polarization dynamics of coexisting CSs and the group-velocity-mismatch affections are also investigated [26]. The spontaneous symmetry breaking (SSB) of two coexisting CSs [27] and the breathing dynamics [28] have been proved by Xu *et al.* The interplay and coupling between the two orthogonal polarization eigenstates with a negligible group-velocity mismatch tends to introduce a strong bound state [29,30]. In addition, similar polarization effects within F-P resonators have also been extensively discussed [31–33]. In this scenario, one would naturally wonder whether the polarization bound states can be flexibly controlled to achieve coupling and decoupling.

In this paper, we propose a birefringent fiber ring with two segments of polarization-maintaining fibers spliced together with a 90° rotation of polarization axes. The intracavity dynamics are investigated in terms of zero and nonzero net birefringence. The coexistence of homogeneous and inhomogeneous states is observed, encompassing the coexistence of modulation instability (MI) patterns (both stable and unstable) with CSs exhibiting both stable and breathing behaviors. Our analysis indicates that adjusting the length difference of the two fibers allows flexible control over the difference in repetition rate of the polarization-multiplexed CSs. At the same time, the number of coexistence states is determined by the detuning difference between the two polarizations. Our investigations within a strongly birefringent resonator shed light on the generation of manageable polarization-multiplexed CSs.

II. THEORETICAL MODEL AND ANALYSIS

We consider the typical polarization-maintaining fiber at 1550 nm, which supports two orthogonal polarization modes expressed as E_1 and E_2, respectively. As shown in Fig. 1, two segment fibers are spliced together with a 90° rotation to exchange the optical fields between two polarizations.

The evolution of the slowly varying intracavity optical field envelopes $E_{1,2}$ of each polarization mode can be described

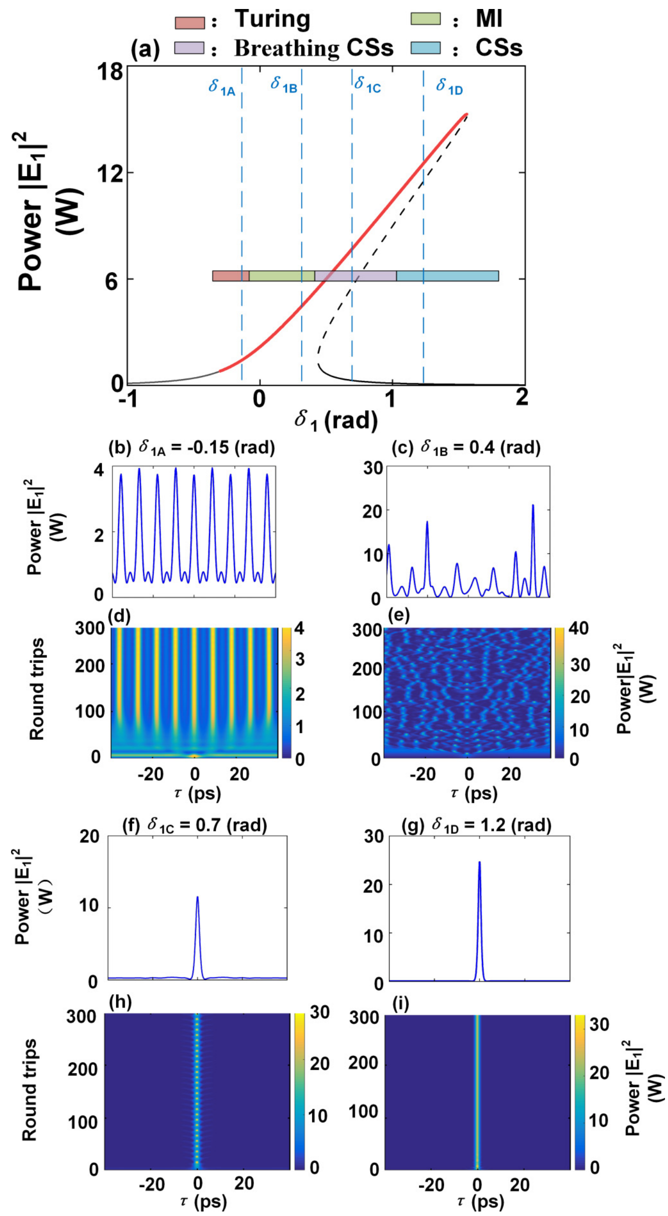

FIG. 2. Cavity resonances and observation of nonlinear states calculated for $\alpha = 7.622 \times 10^{-4}\,\mathrm{m}^{-1}$, $\gamma = 1.2 \times 10^{-3}\,\mathrm{m}^{-1}\,\mathrm{W}^{-1}$, $\theta = 0.05$, $\beta_2 = -2 \times 10^{-26}\,\mathrm{s}^2/\mathrm{m}$, and $\rho = 0.03$. (a) The intracavity power $|E_1|^2$ corresponding to the cw steady-state solutions of Eq. (1). Solid black lines correspond to stable solutions, black dotted lines to homogeneously unstable solutions, and the solid red lines represent MI unstable solutions. (b), (c), (f), (g) Polarization field profiles at various detunings [blue dashed-dotted vertical lines in (a)]. (d), (e), (h), (i) The time-domain evolution of the optical field within 300 round trips corresponding to (b), (c), (f), (g). (b) Turing rolls, $\delta_{1A} = -0.15$ rad; (c) MI patterns, $\delta_{1B} = 0.4$ rad; (f) breathing CS, $\delta_{1C} = 0.7$ rad; (g) CS, $\delta_{1D} = 1.2$ rad.

by two coupled mean-field Lugiato-Lefever equations (LLEs) [34],

$$t_{\mathrm{R}1}\frac{\partial E_1}{\partial t} = \left[-(\alpha_1 + i\delta_1) + i\gamma L(|E_1|^2 + B|E_2|^2) - iL\frac{\beta_2}{2}\frac{\partial^2 E_1}{\partial \tau^2}\right]E_1 + \sqrt{\theta}E_{\mathrm{in}}\cos(\varphi), \tag{1}$$

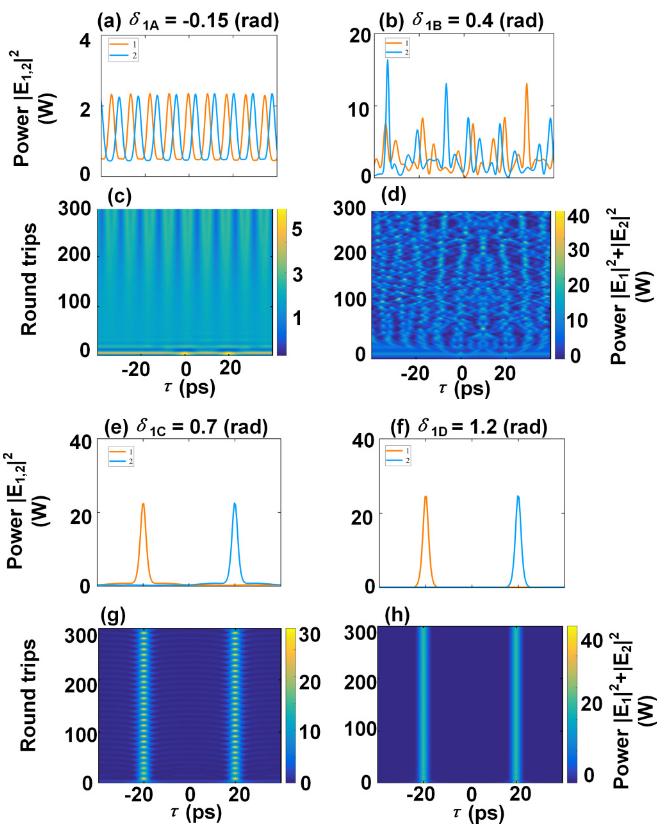

FIG. 3. The time-domain evolution of the nonlinear coexistence states in a zero birefringent resonator. (a), (b), (e), (f) Polarization field profiles at various detunings (same as in Fig. 2). (c), (d), (g), (h) The time-domain evolution of the optical field within 300 round trips corresponding to (a), (b), (e), (f). (a) Two different Turing rolls, $\delta_{1A} = -0.15$ rad; (b) two different MI patterns, $\delta_{1B} = 0.4$ rad; (e) two different breathing CSs, $\delta_{1C} = 0.7$ rad; (f) two different CSs, $\delta_{1D} = 1.2$ rad.

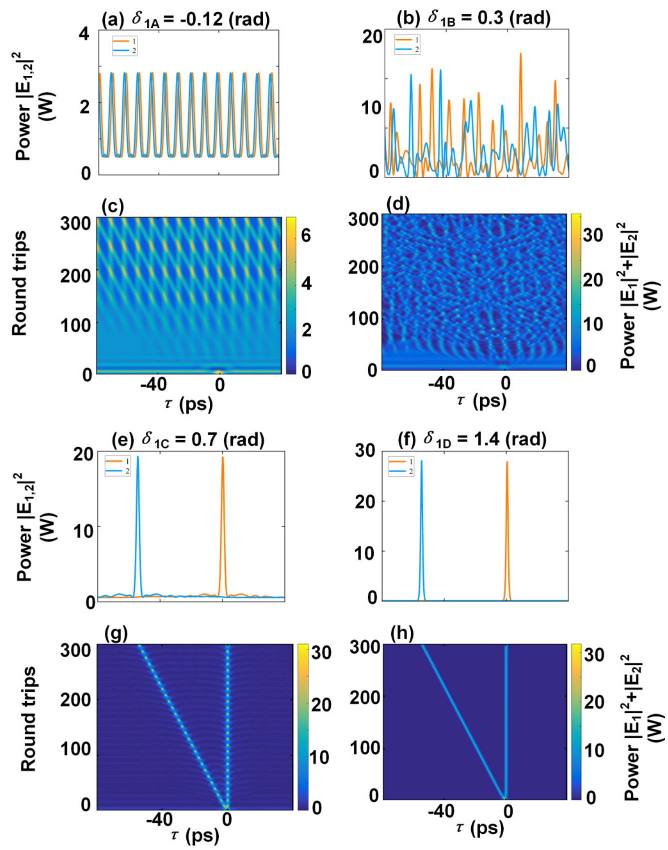

FIG. 4. The time-domain evolution of the nonlinear coexistence states when the detuning difference $\Delta\delta = 2\pi n$. (a), (b), (e), (f) Polarization field profiles at various detunings. (c), (d), (g), (h) The time-domain evolution of the optical field within 300 round trips corresponding to (a), (b), (e), (f). (a) Two different Turing rolls, $\delta_{1A} = -0.12$ rad; (b) two different MI patterns, $\delta_{1B} = 0.3$ rad; (e) two different breathing CSs, $\delta_{1C} = 0.7$ rad; (f) two different CSs, $\delta_{1D} = 1.4$ rad. (Note that the Turing rolls, breathing CS, and CS generated in polarization mode 2 exhibit a temporal delay.)

$$t_{R1}\frac{\partial E_2}{\partial t} = \bigg[-(\alpha_1 + i\delta_2) + i\gamma L(|E_2|^2 + B|E_1|^2) - \eta(t)L\Delta\beta_1\frac{\partial E_2}{\partial \tau} - iL\frac{\beta_2}{2}\frac{\partial^2 E_2}{\partial \tau^2}\bigg]E_2 + \sqrt{\theta}E_{in}\sin(\varphi), \tag{2}$$

where t_{R1} is the roundtrip time of polarization mode 1, and the terms on the right-hand side of Eqs. (1) and (2) indicate the loss, detuning, self-phase modulation, cross-phase modulation (XPM), group-velocity dispersion (GVD), and coherent driving, in turn. $\alpha_1 = [\alpha - lg(1-\theta-2\rho)]/2$ is the total loss, where θ is the power coupling coefficient, and ρ is the power loss coefficient at the splices. δ_1 and δ_2 are the detuning between the monochromatic driving laser and each of the polarization resonances (the order l, the period 2π), which can be expressed as $\delta_1 = 2\pi l - (\beta_{0u}L_1 + \beta_{0v}L_2)$, $\delta_2 = 2\pi l - (\beta_{0u}L_2 + \beta_{0v}L_1)$, respectively, where β_{0u} and β_{0v} are the propagation constant, L_1 and L_2 are the lengths of two segment fibers (thus $\Delta\delta = \delta_1 - \delta_2 = 2\pi\Delta L/L_B$, where L_B is the polarization beat length), and γ is the Kerr nonlinearity coefficient, B is the XPM coefficient of the two polarization modes ($B = 2/3$ for linear birefringence fiber), $\eta(t)$ takes the value of ± 1 (the change of sign indicates the switching of the two polarization modes), $\Delta\beta_1$ denotes the differential group delay (DGD), τ is the fast time, β_2 is the GVD coefficient, and φ denotes the polarization ellipticity. In the context of small driving field and detuning, we can omit the effects of the stimulated Raman scattering (SRS) [35,36].

We first consider exciting one polarization eigenstate to display the typical nonlinear states sustained by the Kerr resonator ($B = 0$). In the following simulations, we set $L = 85$ m, $t_{R1} = 418.41$ ns, and $L_B = 5 \times 10^{-3}$ m. Figure 2(a) shows the predicted intracavity power $|E_1|^2$ varying with δ_1, which is obtained by solving the cw steady-state solutions of Eq. (1). As shown in Fig. 2(a), distinct detuning regions correspond to different nonlinear states, including the Turing rolls (red rectangle), MI patterns (green rectangle), breathing CS (purple rectangle), and CS (blue rectangle). The polarization temporal profiles at various detunings are depicted in Figs. 2(b), 2(c), 2(f), and 2(g), corresponding to the blue dashed-dotted vertical lines in Fig. 2(a). Additionally, the pseudocolor plots

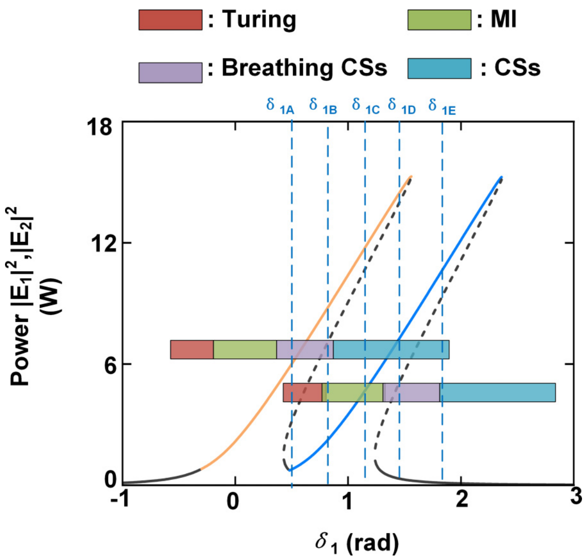

FIG. 5. The intracavity power ($|E_1|^2$, $|E_2|^2$) corresponding to the cw steady-state solutions of Eqs. (1) and (2).

in Figs. 2(d), 2(e), 2(h), and 2(i) show the corresponding time-domain evolution of the optical field within 300 round trips.

III. NONLINEAR STATES COEXISTENCE

A. Zero net birefringence

In order to observe the coexistence of nonlinear states within the resonator, two orthogonal polarizations are considered. We explore one scenario in which the resonator has zero net birefringence, indicating the length difference of the two fibers is zero ($\Delta L = 0$). Figures 3(a), 3(b), 3(e), and 3(f) show the coexistence of homogeneous nonlinear states at the same detuning δ_1 as those in Fig. 2. This occurs because the detuning and length differences of the two polarizations satisfy the condition of $\Delta\delta = \delta_1 – \delta_2 = 2\pi\Delta L/L_B$. Their coinciding resonances result in the excitation of homogeneous coexistence states. Additionally, the relative positions of the two optical fields in the time domain remain unchanged at the end of each round trip due to the equal round-trip time of the two polarizations, which is consistent with the phenomenon shown in Figs. 3(g) and 3(h).

B. Nonzero net birefringence and the detuning difference $\Delta\delta = 2\pi n$

In another scenario, a nonzero fiber length difference ($\Delta L \neq 0$) results in a nonzero net birefringence in the resonator. The resonances of the two polarizations, corresponding to different orders, can coincide when the condition $\Delta L = nL_B$ (n is a positive integer) is met. Therefore, there are two situations to be discussed separately according to whether or not the detuning difference $\Delta\delta$ is a multiple of 2π. Firstly, assuming $\Delta\delta = 2\pi n$, the homogeneous coexistence states shown in Fig. 4 are akin to those depicted in Fig. 3. In contrast to Fig. 3, the presence of $\Delta L = nL_B \neq 0$ introduces a proportional delay in the time domain for Turing rolls, breathing CS, and CS generated in polarization mode 2, as shown in Figs. 4(c), 4(g), and 4(h).

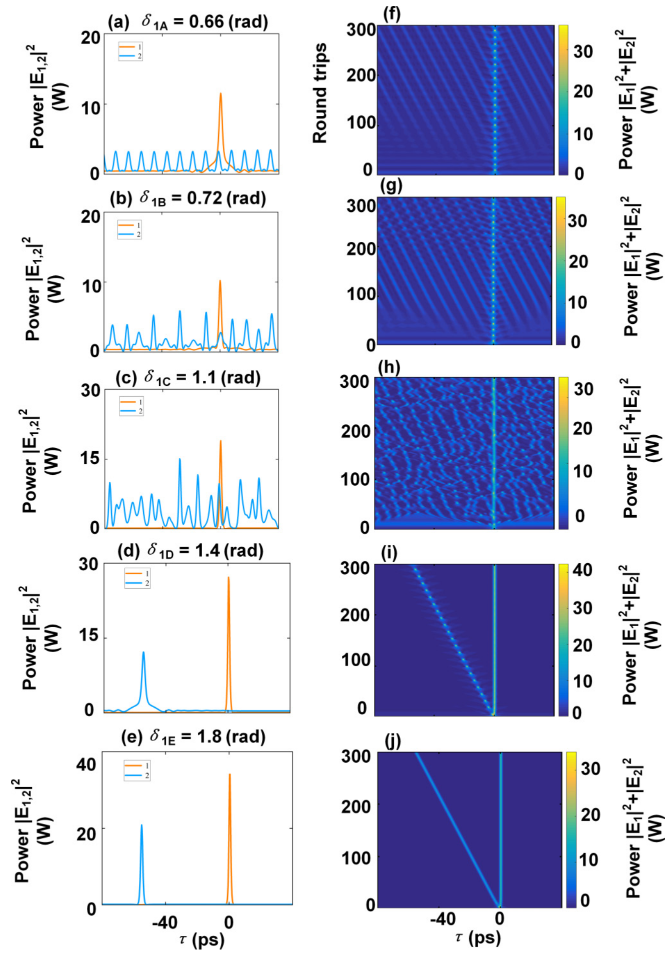

FIG. 6. The time-domain evolution of the nonlinear coexistence states when the detuning difference $\Delta\delta \neq 2\pi n$: $\Delta\delta = 0.8$ rad and $\Delta L = 9.0637 \times 10^{-2}$ m. (a)–(e) Polarization field profiles at various detunings (blue dashed-dotted vertical lines in Fig. 5). (f)–(j) The time-domain evolution of the optical field within 300 round trips corresponding to (a)–(e). (a) Turing rolls and breathing CS, $\delta_{1A} = 0.66$ rad; (b) MI pattern and breathing CS, $\delta_{1B} = 0.72$ rad; (c) MI pattern and CS, $\delta_{1C} = 1.1$ rad; (d) breathing CS and CS, $\delta_{1D} = 1.4$ rad; (e) two different CSs, $\delta_{1E} = 1.8$ rad.

C. Nonzero net birefringence and the detuning difference $\Delta\delta \neq 2\pi n$

Subsequently, the nonlinear coexistence states in a nonzero birefringent resonator are considered when the detuning difference $\Delta\delta \neq 2\pi n$. In this case, the resonances corresponding to the two polarizations exhibit partial overlap. Due to the nonzero birefringence, the two polarizations are associated with different resonant frequencies, and several distinct coexistence states are excited in the resonator. When the detuning difference is $\Delta\delta = 0.8$ rad (corresponding to a length difference of $\Delta L = 9.0637 \times 10^{-2}$ m), the optical power ($|E_1|^2$, $|E_2|^2$) of the two polarizations varying with the detuning δ_1 is depicted in Fig. 5. Furthermore, Fig. 6 shows five distinct coexistence states encompassing both homogeneous and inhomogeneous, such as CS in polarization 1 coexisting with

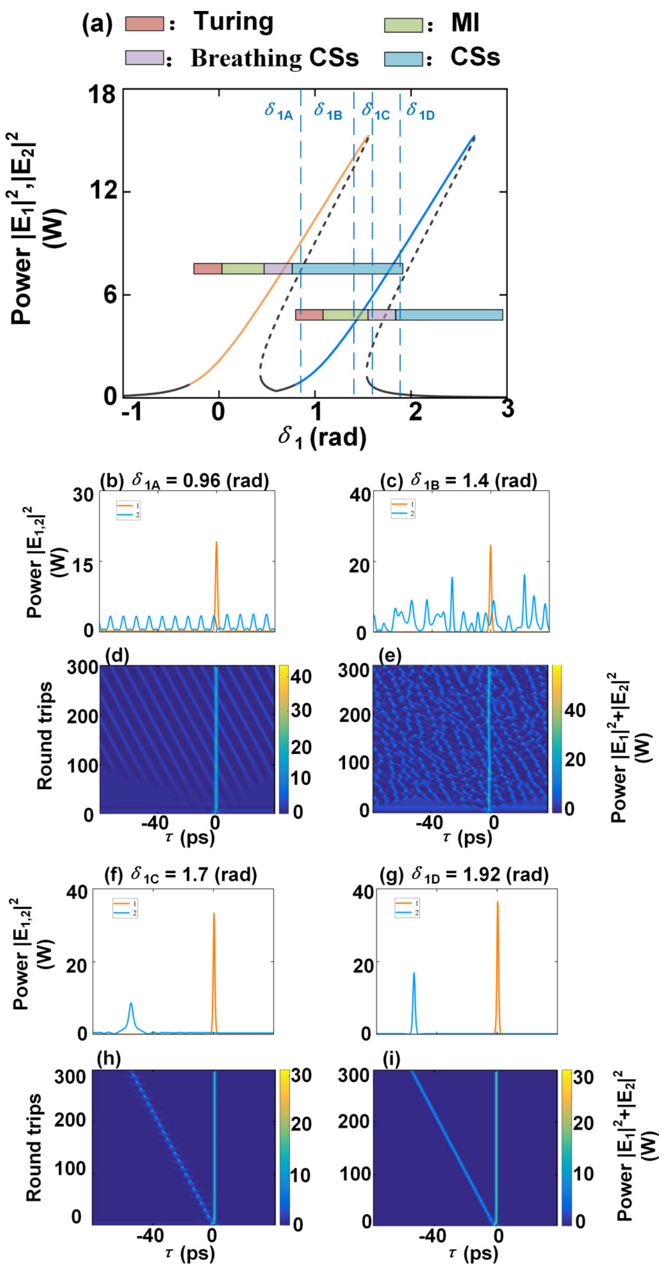

FIG. 7. Cavity resonances and observations of the coexistence of nonlinear states calculated for $\Delta\delta = 1.1$ rad and $\Delta L = 9.0875 \times 10^{-2}$ m: (a) Total intracavity power ($|E_1|^2$, $|E_2|^2$) corresponding to the CW steady-state solutions of Eqs. (1) and (2). (b), (c), (f), (g) Polarization field profiles at various detunings [blue dashed-dotted vertical lines in Fig. 7(a)]. (d), (e), (h), (i) The time-domain evolution of the optical field within 300 round trips corresponding to (b), (c), (f), (g). (b) Turing rolls and CS, $\delta_{1A} = 0.96$ rad; (c) MI pattern and CS, $\delta_{1B} = 1.4$ rad; (f) breathing CS and CS, $\delta_{1C} = 1.7$ rad; (g) two different CSs, $\delta_{1D} = 1.92$ rad.

the aperiodic MI pattern in polarization 2 [Fig. 6(c)] and two polarization CSs with distinct peaks and pulse widths [Fig. 6(e)]. The results are in excellent agreement with the theoretical predictions.

The overlap between the nonlinear states of the two polarizations narrows as the detuning difference increases. As shown in Fig. 7(a), when the detuning difference is $\Delta\delta$=1.1 rad, the overlap region comprises solely the stable CS of polarization mode 1. Four distinct nonlinear states in polarization mode 2 coexisting with the CS in polarization mode 1 are illustrated in Figs. 7(b), 7(c), 7(f), and 7(g).

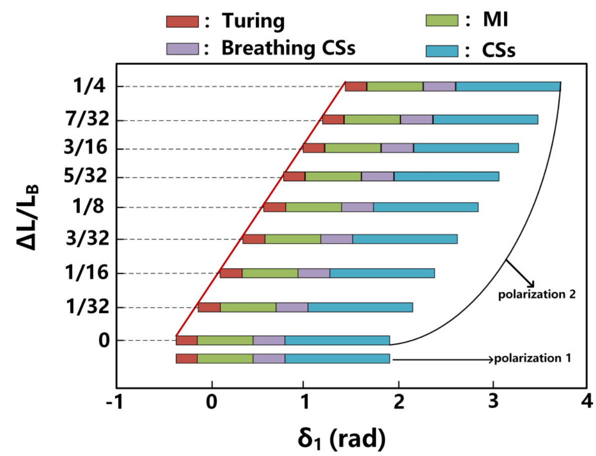

FIG. 8. The field distribution of two polarizations as a function of the difference in fiber length.

As shown in Fig. 8, we further determine the coexistence regions with respect to the detuning δ_1 and the fiber length difference expressed as a fraction of the polarization beat length ($\Delta L/L_B$). The number of distinct coexistence states decreases with the increase of $\Delta L/L_B$. At the same time, the repetition rate difference between the two polarizations also undergoes alteration. Therefore, our findings suggest that the disparity in repetition rates can be flexibly modified by adjusting the length difference ΔL of the two fibers.

IV. DISCUSSION AND CONCLUSIONS

If we look back to the experiment of Anderson *et al.* [24], we may understand that the impact of the Raman effect cannot be simply neglected in the case of high-power pumping to excite the generation of tristability of the resonances and the subsequent supercavity solitons. We may predict that the Raman effect and other high-order nonlinear terms will probably induce the soliton form as well as the drifting trajectory. Here we provide the proof-of-concept demonstration of the coexistence of multiple stable states exhibited on distinct polarizations. However, more quantitative analysis of the rich nonlinear dynamic effects in fiber ring resonators still requires further investigations.

In conclusion, we have investigated the dynamics of distinct polarizations within the strongly birefringent resonator operating in the anomalous dispersion regime. Two segment polarization-maintaining fibers are spliced together with a 90° rotation of polarization axes. Different coexistence of nonlinear states is achievable by varying the length difference of the two fiber sections. The homogeneous coexistence was observed when the length difference was zero. Furthermore, when the nonzero length difference is an integer multiple of the polarization beat length, the homogeneous coexistence was also observed, while the Turing rolls, breathing CS, and CS generated in polarization mode 2 exhibit a temporal delay. In addition, the coexistence of various nonlinear states, such as the CS with the MI pattern (both stable and unstable) and inhomogeneous CSs, is observed when the length difference is not an integer multiple of the polarization beat length. The number of coexistence states varies with the length difference. In particular, two coexisting CSs in different polarizations have been observed. Our findings could have important implications for the generation of polarization-multiplexed dual optical frequency combs.

ACKNOWLEDGMENTS

This work was supported by the Key Research and Development Program of Hubei Province, China (Grant No. 2023BAB062), the Natural Science Foundation of Guangdong Province, China (Grant No. 2023A1515010965), the Technology Innovation Project of Hubei Province, China (Grant No. 2022BEC003), and National Natural Science Foundation of China (Grant No. 62275097).

[1] T. Herr, V. Brasch, J. D. Jost, C. Y. Wang, N. M. Kondratiev, M. L. Gorodetsky, and T. J. Kippenberg, Temporal solitons in optical microresonators, Nat. Photonics **8**, 145 (2014).

[2] X. Xue, Y. Xuan, Y. Liu, P. Wang, S. Chen, J. Wang, D. E. Leaird, M. Qi, and A. M. Weiner, Mode-locked dark pulse Kerr combs in normal-dispersion microresonators, Nat. Photonics **9**, 594 (2015).

[3] X. Liu, C. Sun, B. Xiong, L. Wang, J. Wang, Y. Han, Z. Hao, H. Li, Y. Luo, J. Yan *et al.*, Generation of multiple near-visible comb lines in an AlN microring via $\chi(2)$ and $\chi(3)$ optical nonlinearities, Appl. Phys. Lett. **113**, 171106 (2018).

[4] E. Obrzud, S. Lecomte, and T. Herr, Temporal solitons in microresonators driven by optical pulses, Nat. Photonics **11**, 600 (2017).

[5] T. Fortier and E. Baumann, 20 years of developments in optical frequency comb technology and applications, Commun. Phys. **2**, 153 (2019).

[6] K. Minoshima and H. Matsumoto, High-accuracy measurement of 240-m distance in an optical tunnel by use of a compact femtosecond laser, Appl. Opt. **39**, 5512 (2000).

[7] P. Trocha, M. Karpov, D. Ganin, M. H. P. Pfeiffer, A. Kordts, S. Wolf, J. Krockenberger, P. Marin-Palomo, C. Weimann, S. Randel *et al.*, Ultrafast optical ranging using microresonator soliton frequency combs, Science **359**, 887 (2018).

[8] M. T. Murphy, T. Udem, R. Holzwarth, A. Sizmann, L. Pasquini, C. Araujo-Hauck, H. Dekker, S. D'Odorico, M. Fischer, T. W. Haensch *et al.*, High-precision wavelength calibration of astronomical spectrographs with laser frequency combs, Mon. Not. R. Astron. Soc. **380**, 839 (2007).

[9] Z. L. Newman, V. Maurice, T. Drake, J. R. Stone, T. C. Briles, D. T. Spencer, C. Fredrick, Q. Li, D. Westly, B. R. Ilic *et al.*, Architecture for the photonic integration of an optical atomic clock, Optica **6**, 680 (2019).

[10] V. Torres-Company and A. M. Weiner, Optical frequency comb technology for ultra-broadband radio-frequency photonics, Laser Photonics Rev. **8**, 368 (2014).

[11] F. C. Cruz, D. L. Maser, T. Johnson, G. Ycas, A. Klose, F. R. Giorgetta, I. Coddington, and S. A. Diddams, Mid-infrared optical frequency combs based on difference frequency generation for molecular spectroscopy, Opt. Express **23**, 26814 (2015).

[12] D. C. Cole, A. Gatti, S. B. Papp, F. Prati, and L. Lugiato, Theory of Kerr frequency combs in Fabry-Perot resonators, Phys. Rev. A **98**, 013831 (2018).

[13] F. Leo, S. Coen, P. Kockaert, S. P. Gorza, P. Emplit, and M. Haelterman, Temporal cavity solitons in one-dimensional Kerr media as bits in an all-optical buffer, Nat. Photonics **4**, 471 (2010).

[14] C. Bao and C. Yang, Stretched cavity soliton in dispersion-managed Kerr resonators, Phys. Rev. A **92**, 023802 (2015).

[15] A. U. Nielsen, B. Garbin, S. Coen, S. G. Murdoch, and M. Erkintalo, Invited article: Emission of intense resonant radiation by dispersion-managed Kerr cavity solitons, APL Photonics **3**, 120804 (2018).

[16] X. Xue, P. Grelu, B. Yang, M. Wang, S. Li, X. Zheng, and B. Zhou, Dispersion-less Kerr solitons in spectrally confined optical cavities, Light: Sci. Appl. **12**, 19 (2023).

[17] N. Englebert, C. Mas Arabí, P. Parra-Rivas, S. P. Gorza, and F. Leo, Temporal solitons in a coherently driven active resonator, Nat. Photonics **15**, 536 (2021).

[18] J. Pan, T. Huang, Y. Wang, Z. Wu, J. Zhang, and L. Zhao, Numerical investigations of cavity-soliton distillation in Kerr resonators using the nonlinear Fourier transform, Phys. Rev. A **104**, 043507 (2021).

[19] J. Pan, Z. Cheng, T. Huang, M. Zhu, Z. Wu, and P. P. Shum, Numerical investigation of all-optical manipulation for polarization-multiplexed cavity solitons, J. Lightwave Technol. **39**, 582 (2020).

[20] N. Englebert, N. Goldman, M. Erkintalo, N. Mostaan, S. P. Gorza, F. Leo, and J. Fatome, Bloch oscillations of coherently driven dissipative solitons in a synthetic dimension, arXiv:2112.10756.

[21] Y. Sun, P. Parra-Rivas, C. Milián, Y. V. Kartashov, M. Ferraro, F. Mangini, R. Jauberteau, F. R. Talenti, and S. Wabnitz, Robust three-dimensional high-order solitons and breathers in driven dissipative systems: A Kerr cavity realization, Phys. Rev. Lett. **131**, 137201 (2023).

[22] R. Chen, H. Shu, B. Shen, L. Chang. W. Xie, W. Liao, Z. Tao, J. E. Bowers, and X. Wang, Breaking the temporal and frequency congestion of LiDAR by parallel chaos, Nat. Photonics **17**, 306 (2023).

[23] B. Shen, H. Shu, W. Xie, R. Chen, Z. Liu, Z. Ge, X. Zhang, Y. Wang, Y. Zhang, B. Cheng *et al.*, Harnessing microcomb-based parallel chaos for random number generation and optical decision making, Nat. Commun. **14**, 4590 (2023).

[24] M. Anderson, Y. Wang, F. Leo, S. Cohen, M. Erkintalo, and S. G. Murdoch, Coexistence of multiple nonlinear states in a tristable passive Kerr resonator, Phys. Rev. X **7**, 031031 (2017).

[25] A. U. Nielsen, B. Garbin, S. Coen, S. G. Murdoch, and M. Erkintalo, Coexistence and interactions between nonlinear states with different polarizations in a monochromatically driven passive Kerr resonator, Phys. Rev. Lett. **123**, 013902 (2019).

[26] M. Saha, S. Roy, and S. K. Varshney, Polarization dynamics of a vector cavity soliton in a birefringent fiber resonator, Phys. Rev. A **101**, 033826 (2020).

[27] G. Xu, A. U. Nielsen, B. Garbin, L. Hill, G.-L. Oppo, J. Fatome, S. G. Murdoch, S. Coen, and M. Erkintalo, Spontaneous symmetry breaking of dissipative optical solitons in a two-component Kerr resonator, Nat. Commun. **12**, 4023 (2021).

[28] G. Xu, L. Hill, J. Fatome, G.-L. Oppo, M. Erkintalo, S. G. Murdoch, and S. Coen, Breathing dynamics of symmetry-broken temporal cavity solitons in Kerr ring resonators, Opt. Lett. **47**, 1486 (2022).

[29] J. Pan, Z. Cheng, T. Huang, C. Long, P. P. Shum, and G. Brambilla, Fundamental and third harmonic mode coupling induced single soliton generation in Kerr microresonators, J. Lightwave Technol. **37**, 5531 (2019).

[30] S. Feng, Y. Yao, P. P. Shum, G. Xu, J. Pan, C. Xu, Z. Wu, J. Zhang, X. Li, L. Han *et al.*, Cavity soliton in a cyclic polarization permutation fiber resonator, Opt. Express **30**, 46900 (2022).

[31] L. Hill, E. M. Hirmer, G. Campbell, T. Bi, A. Ghosh, P. Del'Haye, and G.-L. Oppo, Symmetry broken vectorial Kerr frequency combs from Fabry-Pérot resonators, arXiv:2308.05039.

[32] N. Moroney, L. Del. Bino, S. Zhang, M. T. M. Woodley, L. Hill, T. Wildi, V. J. Wittwer, T. Sudmeyer, G.-L. Oppo, M. R. Vanner *et al.*, A Kerr polarization controller, Nat. Commun. **13**, 398 (2022).

[33] G. N. Campbell, L. Hill, P. Del'Haye, and G.-L. Oppo, Dark temporal cavity soliton pairs in Fabry-Pérot resonators with normal dispersion and orthogonal polarizations, in *2023 Conference on Lasers and Electro-Optics Europe & European Quantum Electronics Conference* (CLEO/Europe-EQEC, IEEE, New York, 2023), p. 1.

[34] E. Averlant, M. Tlidi, K. Panajotov, and L. Weicker, Coexistence of cavity solitons with different polarization states and different power peaks in all-fiber resonators, Opt. Lett. **42**, 2750 (2017).

[35] Y. Wang, M. Anderson, S. Coen, S. G. Murdoch, and M. Erkintalo, Stimulated Raman scattering imposes fundamental limits to the duration and bandwidth of temporal cavity solitons, Phys. Rev. Lett. **120**, 053902 (2018).

[36] M. Karpov, H. Guo, A. Kordts, V. Brasch, M. H. P. Pfeiffer, M. Zervas, M. Geiselmann, and T. J. Kippenberg, Raman self-frequency shift of dissipative Kerr solitons in an optical microresonator, Phys. Rev. Lett. **116**, 103902 (2016).